The following article appeared in *Journal of Volcanology and Geothermal Research, Volume 324, 2018, Pages 15-27;* and may be found at: https://doi.org/10.1016/j.jvolgeores.2016.05.006

Journal of Volcanology and Geothermal Research 324 (2016) 15–27

Contents lists available at ScienceDirect

Journal of Volcanology and Geothermal Research

journal homepage: www.elsevier.com/locate/jvolgeores

Internal architecture of the Tuxtla volcanic field, Veracruz, Mexico, inferred from gravity and magnetic data

Juan Manuel Espindola [a,*], Hector Lopez-Loera [b], Manuel Mena [a], Araceli Zamora-Camacho [c]

[a] Instituto de Geofísica, Universidad Nacional Autónoma de México, Ciudad Universitaria, Ciudad de México, C.P. 04510, Mexico
[b] División de Geociencias Aplicadas, Instituto Potosino de Investigación Científica y Tecnológica, Camino a la Presa San José 2055, Col. Lomas 4a sección, San Luis Potosí, C.P. 78216 S.L.P., Mexico
[c] Centro de Sismología y Vulcanología de Occidente, Centro Universitario de la Costa. Universidad de Guadalajara, Av. Universidad 203, Delegación Ixtapa, Puerto Vallarta, C.P.48280, Jalisco, Mexico

ARTICLE INFO

Article history:
Received 26 October 2015
Received in revised form 11 May 2016
Accepted 12 May 2016
Available online 14 May 2016

Keywords:
Tuxtla volcanic field
Basaltic volcanic fields
Magmatic processes
Potential signals in volcanic areas
Volcanoes of Mexico

ABSTRACT

The Tuxtla Volcanic Field (TVF) is a basaltic volcanic field emerging from the plains of the western margin of the Gulf of Mexico in the Mexican State of Veracruz. Separated by hundreds of kilometers from the Trans-Mexican Volcanic Belt to the NW and the Chiapanecan Volcanic Arc to the SE, it stands detached not only in location but also in the composition of its rocks, which are predominantly alkaline. These characteristics make its origin somewhat puzzling. Furthermore, one of the large volcanoes of the field, San Martin Tuxtla, underwent an eruptive period in historical times (CE 1793). Such volcanic activity conveys particular importance to the study of the TVF from the perspective of volcanology and hazard assessment. Despite the above circumstances, few investigations about its internal structure have been reported. In this work, we present analyses of gravity and aeromagnetic data obtained from different sources. We present the complete Bouguer anomaly of the area and its separation into regional and residual components. The aeromagnetic data were processed to yield the reduction to the pole, the analytic signal, and the upward continuation to complete the interpretation of the gravity analyses. Three-dimensional density models of the regional and residual anomalies were obtained by inversion of the gravity signal adding the response of rectangular prisms at the nodes of a regular grid. We obtained a body with a somewhat flattened top at 16 km below sea level from the inversion of the regional. Three separate slender bodies with tops 6 km deep were obtained from the inversion of the residual. The gravity and magnetic anomalies, as well as the inferred source bodies that produce those geophysical anomalies, lie between the Sontecomapan and Catemaco faults, which are proposed as flower structures associated with an inferred deep-seated fault termed the Veracruz Fault. These fault systems along with magma intrusion at the lower crust are necessary features to understand the origin and structure of the TVF.

1. Introduction

The Tuxtla Volcanic Field (TVF), also known as Los Tuxtlas Volcanic Field or Los Tuxtlas Massif, is an isolated basaltic field emerging from the lowlands of the western margin of the Gulf of Mexico. It lies in the Veracruz Basin, in the Mexican State of Veracruz (Fig. 1) 230 km to the SSE of the easternmost tip of the Trans-Mexican Volcanic Belt (TMVB), and about the same distance from El Chichon volcano to the SE, in the Chiapanecan Volcanic Arc. Due to its separation from these volcanic chains, as well as to the alkaline composition of its rocks, the origin of this volcanic field has been an intriguing question for many investigators of the Mexican geology (e.g. Pichler and Weyl, 1976; Robin, 1976; Thorpe, 1977; Cantagrel and Robin, 1979; Nelson et al., 1995; Verma, 2006). However, until now there is no general agreement on this question (e.g. Nelson et al., 1995; Verma, 2006). The TVF has received less attention than other volcanic areas of Mexico despite being the site of a volcanic eruption in historical times (San Martin Tuxtla volcano, 1773). Nevertheless, because the western margin of the Gulf of Mexico has been widely studied, mostly from the perspective of oil and gas exploration, several geophysical surveys have included the TVF. In particular, the area is marked by conspicuous gravity and geomagnetic anomalies circumscribed to the field. Although these signals had not been analyzed in a volcanological context, they offer insight into the structure of this volcanic field. We carried out such analysis aiming to infer the internal fabric of this volcanic field.

* Corresponding author.
E-mail address: jmec@unam.mx (J.M. Espindola).

http://dx.doi.org/10.1016/j.jvolgeores.2016.05.006

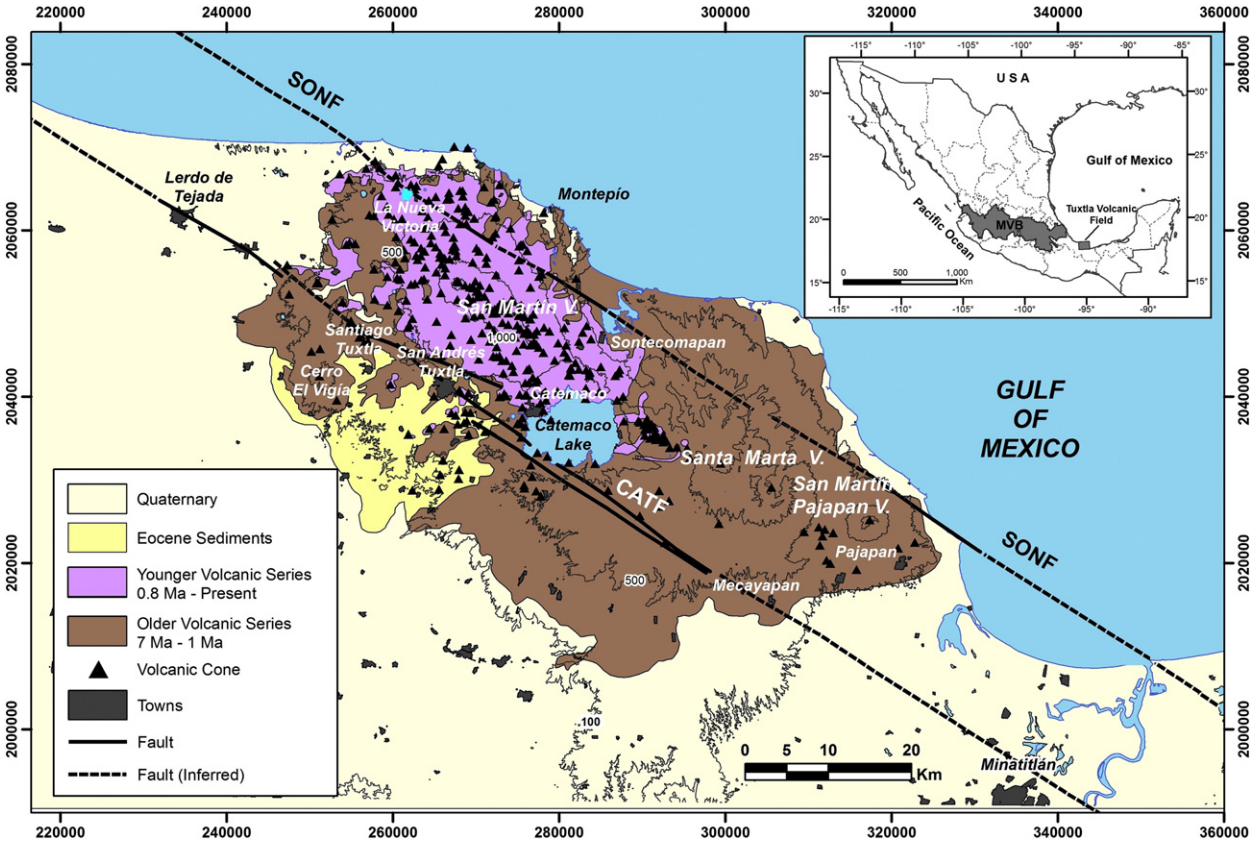

Fig. 1. Location of the Tuxtla Volcanic Field (inset). Generalized Geologic and structural map of Los Tuxtlas Volcanic Field. Continuous lines: faults; dashed lines: inferred faults. CATF: Catemaco Fault. SONF: Sontecomapan Fault.
Geology after Nelson and Gonzalez-Caver (1992); faults after Andreani et al. (2008).

2. Geology and tectonic setting

The TVF lies in the middle of the Veracruz Basin; a Tertiary NNW trending basin extending from the eastern tip of the Transmexican Volcanic Belt to the Salina del Istmo Basin (Padilla y Sánchez, 2007). It lies approximately 230 km from the tip of the Trans-Mexican volcanic belt (TMVB) and El Chichon volcano to the SE and 350 km from the closest point on the Pacific trench. The subducting slab beneath this region, if present, is much deeper than 150 km as judging from the extrapolation of seismic foci. Analyses of receiver functions yield no evidence of the subducted plate interface (Espíndola, 2009; Melgar and Perez-Campos, 2010), although recently Kim et al. (2011) also based on receiver functions, interpreted some phases as transformed at the interphase with a relic slab some 50 km below the TVF. They propose that it was the result subduction of oceanic lithosphere, before the collision of the Yucatán Block with Mexico, about 12 Ma ago.

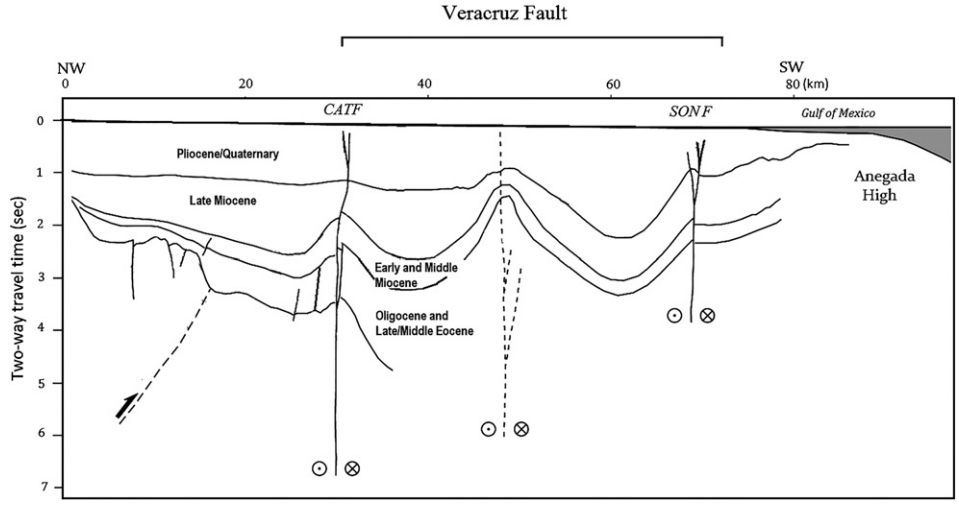

Fig. 2. Cross section across the Veracruz Basin (about 100 km NW from the TVF) based on seismic reflection data. The horizontal axis is the distance in kilometers; the vertical axis is two-way travel time in seconds. CATF: Catemaco Fault. SONF: Sontecomapan Fault.
Modified after Andreani et al. (2008).

Table 1
Equipment, procedures, and treatment of the geomagnetic data provided by the Servicio Geológico Mexicano.

Equipment and instruments	
Plane	Islander BN2-B21; BN2-B27
Fight magnetometer	Scintrex CS-3; Geometrics G-822 A Cesium Opt. Pump
Sensitivity	0.001 nT
Data acquisition system	PICODAS P-101
Base Station magnetometer	GEM systems GSM-19, Overhauser
Sensitivity	0.01 nT
Radar altimetry	TERRA TRI40-TRA3000
Navigation system	GPS ASHTEC + GLONASS
Flight parameters	
Direction of lines of flight	North–south
Distance between flight lines	1000 m
Distance between control lines	10,000 m
Flight altitude	300 m
Navigation	Electronic (GPS)
Data processing	
Correction for plane movement	Magnetic compensation
Reductions	Diurnal variation. Subtraction of the IGRF 2000
Leveling	Control lines, microleveling
Projection	Transverse universal mercator
Grid	UTM every 5000 m
Spheroid	Clarke 1866
Datum	NAD 27
Contour interval	25 nT
Center of chart geomagnetic	Year of Flight: 2004
Field data	Altitude: 0.80 km
	Intensity: 41,152 nT

Melgar and Perez-Campos (2010) found similar depth to the Moho underneath the TVF pointing out to the existence of significant azimuthal variations in the depth estimations. Zamora-Camacho et al. (2010) also used receiver functions to estimate crustal structure underneath three stations deployed around San Martin Tuxtla volcano. They inferred an interface at a depth of about 28 km for rays arriving from the NW, and about 34 km for rays arriving from the east and south, they proposed this interface as the Moho. They also deduced another velocity contrast at depths between 10 (for rays from the NW) and 14 km continental basement and sediments deposited from early Miocene.

2.1. The Veracruz Basin

The Veracruz Basin developed over the eroded structures of the Zongolica fold-thrust belt and extended to the east towards the Gulf of Mexico (Sawyer et al., 1991; Prost and Aranda-Garcia, 2001). The TVF offshore is located at the margin of the Campeche Salt shelf and south of the Laguna Madre-Tuxpan (LMT) shelf, an extensive geologic province that spans the western Gulf of Mexico (Padilla y Sánchez, 2007; Le Roy et al., 2007). Le Roy et al. (2007) carried out a structural analysis of the area based on seismic profiles, digital elevation models, and satellite imagery. The study is focused mostly on the LMT shelf, but it offers information about the regional tectonic and geologic characteristics of the Veracruz Basin. As stated by these authors the basin evolved during the Mesozoic and Cenozoic. In the early Mesozoic, the Mexican margin was divided by rifting into a series of basement blocks separated by a thinned continental crust (Le Roy et al., 2007). During the Jurassic and Cretaceous post-rift subsidence favored the deposition over the basement blocks of platformal carbonates, concurrently basinal carbonates

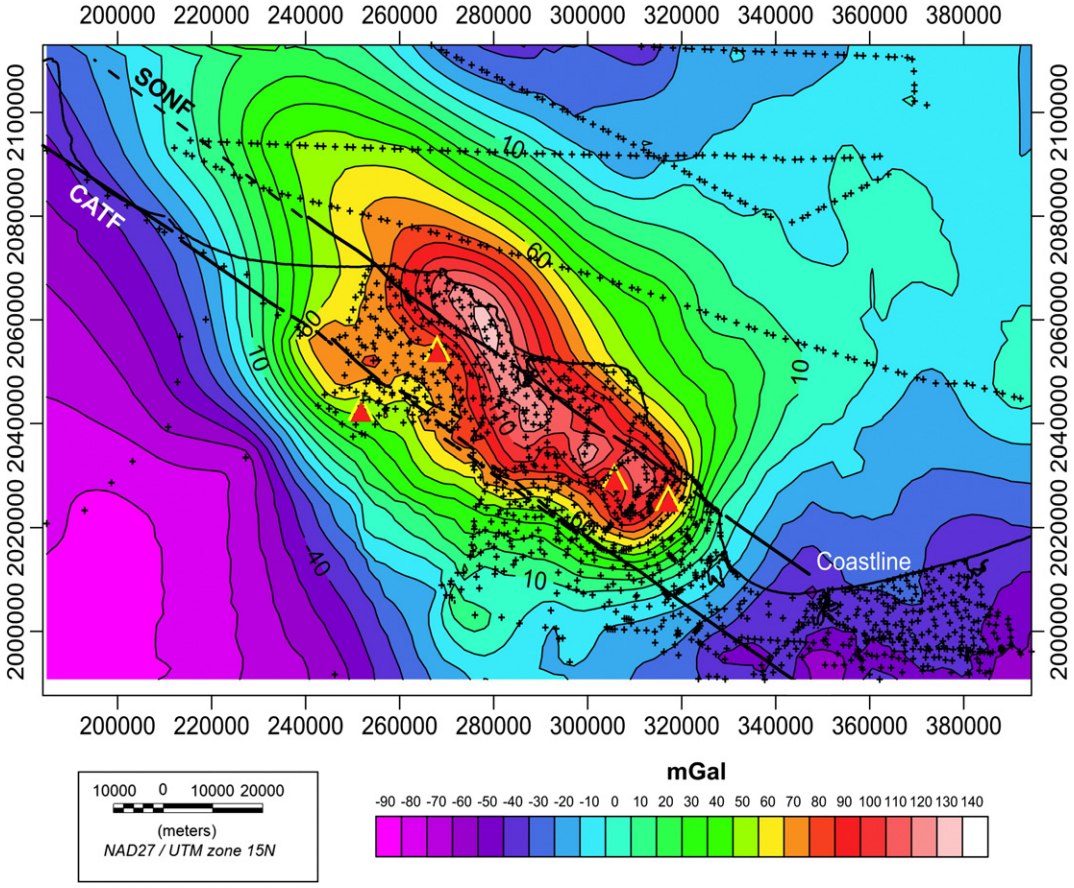

Fig. 3. Complete Bouguer Anomaly. Triangles: Main volcanoes. Small black crosses: gravity stations. Continuous lines: faults; dashed lines: inferred faults.CATF: Catemaco Fault. SONF: Sontecomapan Fault.
Modified after Andreani et al. (2008).

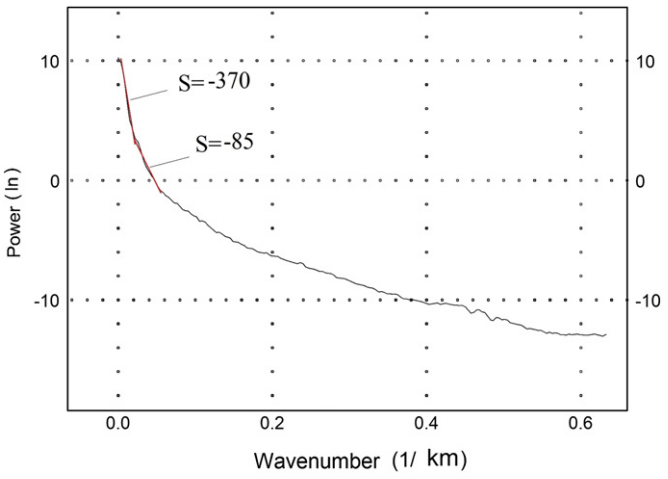

Fig. 4. Radial power spectrum of the gravity signal from the Tuxtla Volcanic Field.

accumulated over areas of thinned crust (Le Roy et al., 2007). During Late Cretaceous–Early Eocene an east-trending thrust belt developed, which formed an emergent thrust fan composed of Cretaceous strata that led to the formation of the western margin of the Veracruz Basin (Le Roy et al., 2007). From the Early Eocene to the present, the emergent thrust belt has delivered sediment to the Veracruz Basin through steep streams (Le Roy et al., 2007). Thus, the depositional setting along the western margin of the basin changes from incised fluvial systems to a deep marine character (Le Roy et al., 2007). Through sedimentation and differential subsidence, the thrust front was buried by more than 8 km of Cenozoic sediments to the east of the basin (Sawyer et al., 1991; Padilla y Sánchez, 2007; Le Roy et al., 2007; Andreani et al., 2008).

Andreani et al. (2008) reported their results on the structural analysis of an area that includes the TVF. From structural data obtained in the field, analysis of satellite images and seismic profiles, they determined that the Veracruz Basin it is affected by at least three NW–SE major left lateral strike-slip faults that continue into the TVF. These NW–SE trending faults are, from north to south, the Sontecomapan fault, the Catemaco fault, and a broad NW trending faulted zone (the Tres Zapotes fault zone). They found that the relationship between topography and faults traces indicated sub-vertical fault planes for these faults. The Sontecomapan fault (Fig. 1) borders the Gulf coast with a surface trace poorly defined. The Catemaco fault is distinct and crosses the entire volcanic field. These faults are parallel to the conspicuous volcanic alignment of the field and are also associated with E–W trending secondary faults that they interpret as synthetic Riedel shears. Finally, these authors propose that the major NW–SE strike-slip faults, identified in the Veracruz Basin and the TVF, merge at depth and form a large transpressive flower structure, which they named the Veracruz Fault. Fig. 2 shows a cross-section, inferred by these authors from gravity modeling and seismic reflection data. The profile is approximately perpendicular to the coastline and the fault's strike, about 100 km NW from the center of the TVF. The figure shows the main fault system cutting the Oligocene and Miocene rocks of the Veracruz Basin. The stratigraphy under the TVF is similar to the latter, with Oligocene, and Miocene rocks under the volcanic rocks of the TVF (Rios Macbeth, 1952). Andreani et al. (2008) found field and indirect

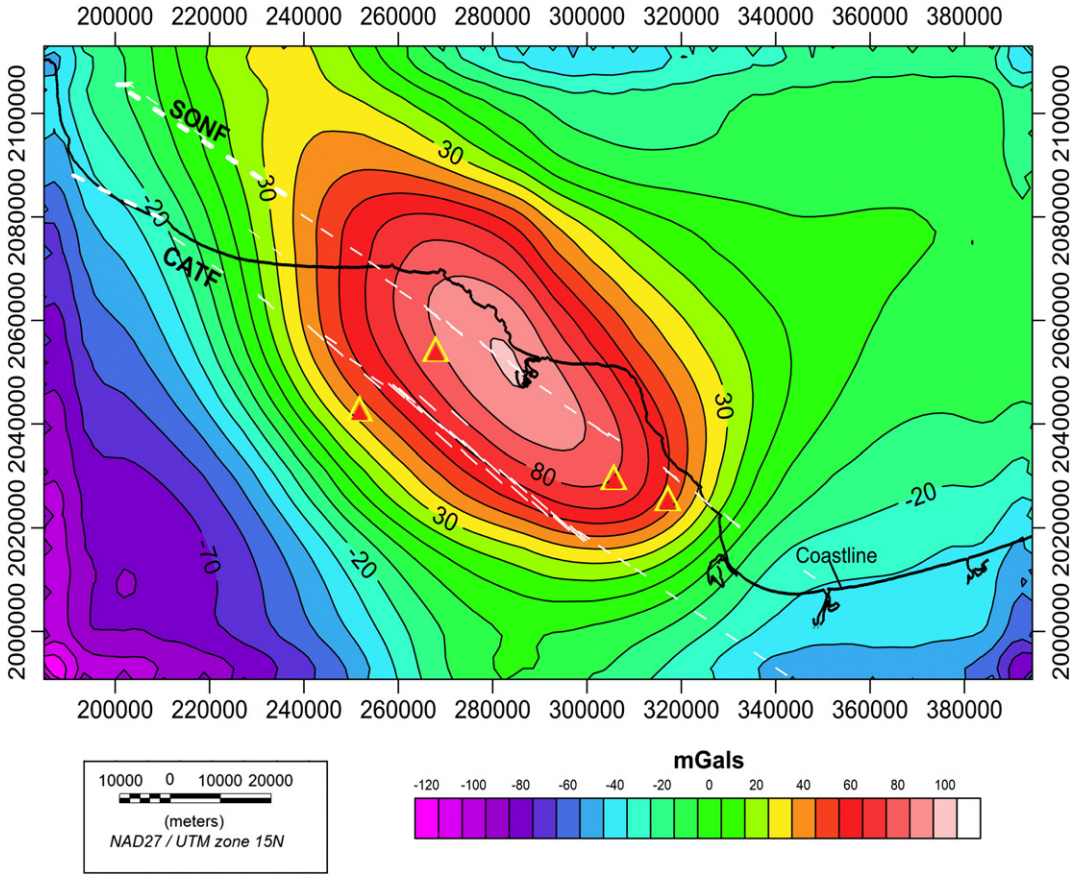

Fig. 5. Regional Bouguer Anomaly. Triangles: Main Volcanoes. Continuous lines: faults; dashed lines: inferred faults. CATF: Catemaco Fault. SONF: Sontecomapan Fault. Modified after Andreani et al. (2008).

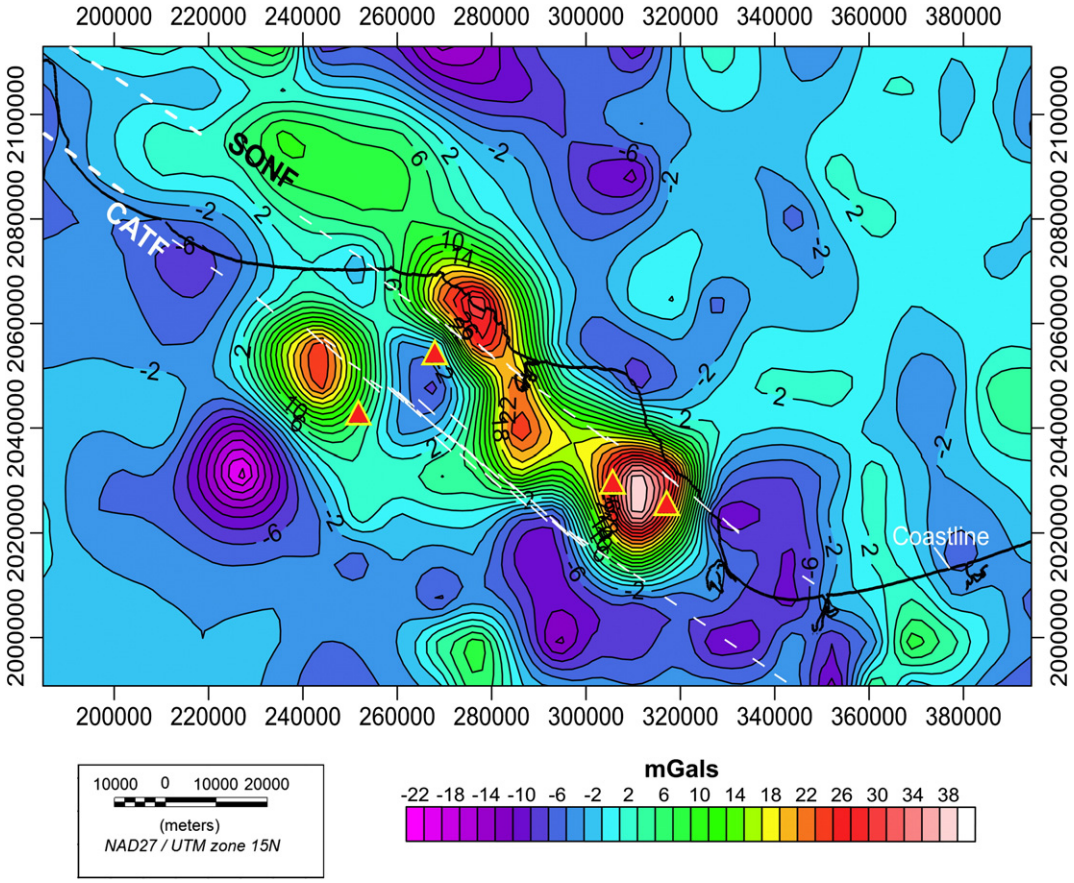

Fig. 6. Residual Bouguer anomaly. Triangles: Main Volcanoes. Continuous lines: faults; dashed lines: inferred faults. CATF: Catemaco Fault. SONF: Sontecomapan Fault. Modified after Andreani et al. (2008).

evidence that the fault system runs across the TVF merging into a single fault beyond the city of Coatzacoalcos a few kilometers SE from the southern edge of the TVF.

2.2. The Tuxtla volcanic field

The structures described above are the framework through which the magmatic rocks of the TVF field were extruded. Andreani et al. (2008) suggest that the evolution of the TVF could be related to the development of the Veracruz fault during the last 5 Ma. The volcanic activity during Late Miocene to Pliocene covered the whole volcanic field and may be associated with several active faults. The rise of magmatic fluids would have been enhanced by the emplacement of small "pull apart" basins, small block rotations, or both. During the Quaternary, the volcanism was linked to a single alignment maybe as the result of the fault localization at depth.

The TVF field spans an area of approximately 2200 km^2 and is composed of primitive basanites, alkali basalts, mildly alkaline Hy-normative mugearites and benmoreites, calc-alkaline basalts, and basaltic andesites (Nelson et al., 1995). These rocks were issued from five large volcanoes (Cerro El Vigía, San Martin Tuxtla, Sierra Santa Marta (composed of Santa Marta and Yohualtapan volcanoes), and San Martin Pajapan, 353 distinct cones, and 42 maars (Fig. 1). Kobs-Nawotniak et al. (2010) carried out a statistical study of the distribution of vents in the TVF. They found that the maars and older cones showed anticlustered distributions indicative of spatial regularity while the youngest division of cones shows clustering in two general groups. The first, broader, group contains V. San Martin Tuxtla, while the smaller, more tightly concentrated group is located east of Lago Catemaco. The eastern group has significantly smaller cones than the rest of the field and is also the site of the densest vent concentration in the TVF, reaching 2 vents per square kilometer.

Aguilera Gómez (1988) and Nelson and Gonzalez-Caver (1992) obtained K–Ar ages of samples from several sites in the volcanic field. From these data, the latter authors concluded that the rocks to the NW of the field are younger (0.8 Ma-present) than the rest of the volcanic field (7 Ma–1.5 Ma). They informally termed those rocks as the Younger and Older volcanic series respectively (Fig. 1). The rocks from these series fall in a broad range of the SiO_2 vs. Alkali plot, going from basanites and picro-basalts to benmoreitas (Nelson et al., 1995). However, the set from the younger series falls mostly in the silica undersaturated range (i.e. picro-basalts and basanites). This characteristic is also found in the tephra and lavas of the 1793 eruption (Espindola et al., 2010). The rocks from the older series, however, are dispersed over the range and include some calc-alkaline rocks. Nelson et al. (1995) found that the primitive magmas resulted from increasing degrees of melting while pressure decreased from greater than 30 kbar to 20 kbar in the garnet stability field. They also determined, in another set of alkali basalts and hawaiites, lower Ni and Cr concentrations and higher Fe/Mg ratios and concluded that they were derived from the primitive group by crystal fractionation at pressures of several kbar. On the origin of the TVF, Nelson et al. (1995) propose that it is related to the subduction of the Cocos plate, and point out the similarities with magmas found in back-arc regions. Other authors, however, have proposed that the TVF is a continuation to the south of the Eastern Alkaline Province (EAP), which is related to the tectonics of the Gulf of Mexico (Robin, 1976; Cantagrel and Robin, 1979). Nevertheless, Nelson et al. (1995) found substantial differences between rocks of both suites and disagree on the belonging of the TVF to the EAP. Furthermore, in a study of the TMVB, Ferrari et al. (2012) propose that a pulse of mafic volcanism migrated from west to east, reaching the Gulf of Mexico by 7 Ma. This age

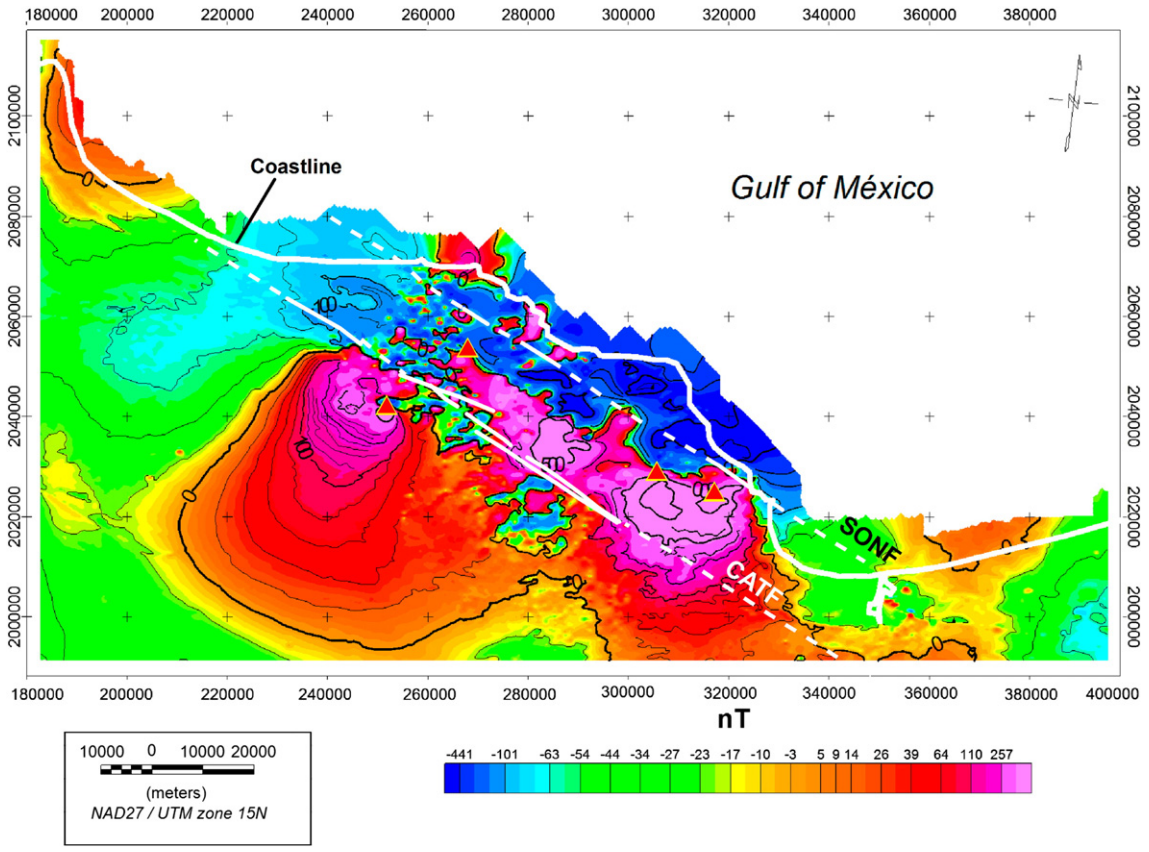

Fig. 7. Residual Magnetic Map of the Tuxtla Volcanic Field. Triangles: Main Volcanoes Continuous lines: faults; dashed lines: inferred faults. CATF: Catemaco Fault. SONF: Sontecomapan Fault.
Modified after Andreani et al. (2008).

coincides with the age of the inception of vulcanism at the TVF, suggesting that the origin of the TVF is linked to the evolution of the nearby TMVB.

3. Data

The gravity data were obtained from the database compiled for the construction of the Gravity Chart of Mexico (De la Fuente et al., 1994). In this database, the information for Los Tuxtlas Region on the continent was contributed by PEMEX the Mexican oil company. The marine data set was one of the products of project CICAR, Cooperative Investigation of the Caribbean and Adjacent Regions (Moore and Del Castillo, 1974). The data consist of the complete Bouguer anomaly reduced with an average density of 2670 kg/m^3 on land and the free air anomaly on the sea. The elevations used were determined using three altimeters tied to the national geodetic network managed by the Instituto Nacional de Estadistica, Geografia e Informatica (INEGI). All the data in the Mexican charts are referred to the world's first order station at Ciudad Universitaria (main campus of the Universidad Nacional Autónoma de Mexico) in Mexico City and associated to the International Gravity Standardization Net 1997 and Geodetic Reference System 1967.

The aeromagnetic data were obtained from the Servicio Geológico Mexicano (SGM), which makes them available to the general public (http://www.sgm.gob.mx). The data were collected with the equipment and procedures shown in Table 1.

4. Methods

4.1. Reduction and transformations of the data

The data were interpolated with a linear variogram kriging method using commercial software (Surfer from Golden Software). The interpolated data were used to obtain a regular grid with nodes separated by 1 km. We separated the gravity anomaly into regional and residual components. The regional was obtained by filtering the data once with a 5 × 5 inverse to the distance low-pass filter using Surfer. The residual was derived by subtraction of the regional from the complete data.

The data provided by the SGM are the Residual Magnetic Field (RMF) attained through subtraction the IGRF-2000 (see Table 1). The RMF was transformed into other signals to facilitate the interpretation. Those transformations yielded:

1) The Reduction to the Pole (RTP), using the mean magnetic field intensity, inclination, and declination for 2004, the year in which the survey was carried out, the values used are listed in Table 1. (e.g. Blakely, 1996; p.330).
2) The Analytic Signal (AS), the amplitude of this signal is the square root of the sum of the squared orthogonal gradients of the total magnetic field. This transformation enhances the edges of the magnetic bodies where the signal peaks (e.g. Blakely, 1996; p.350).
3) The upward continuation to filter high-frequency anomalies caused by shallow sources so as to enhance anomalies caused by deeper sources (Blakely, 1996; p. 313).

Also, for both signals, we obtained the radial power spectrum (RPS), which consists of the spectrum averaged over several azimuths. The RPS is related to the depth (***h***) of a causative body by the relation (e.g. Spector and Grant, 1970; Pal et al., 1979; Dimitriadis et al., 1987):

$$h = \frac{S}{4\pi}$$

where ***s*** is the slope of a line fitted to the data in a plot of the logarithm

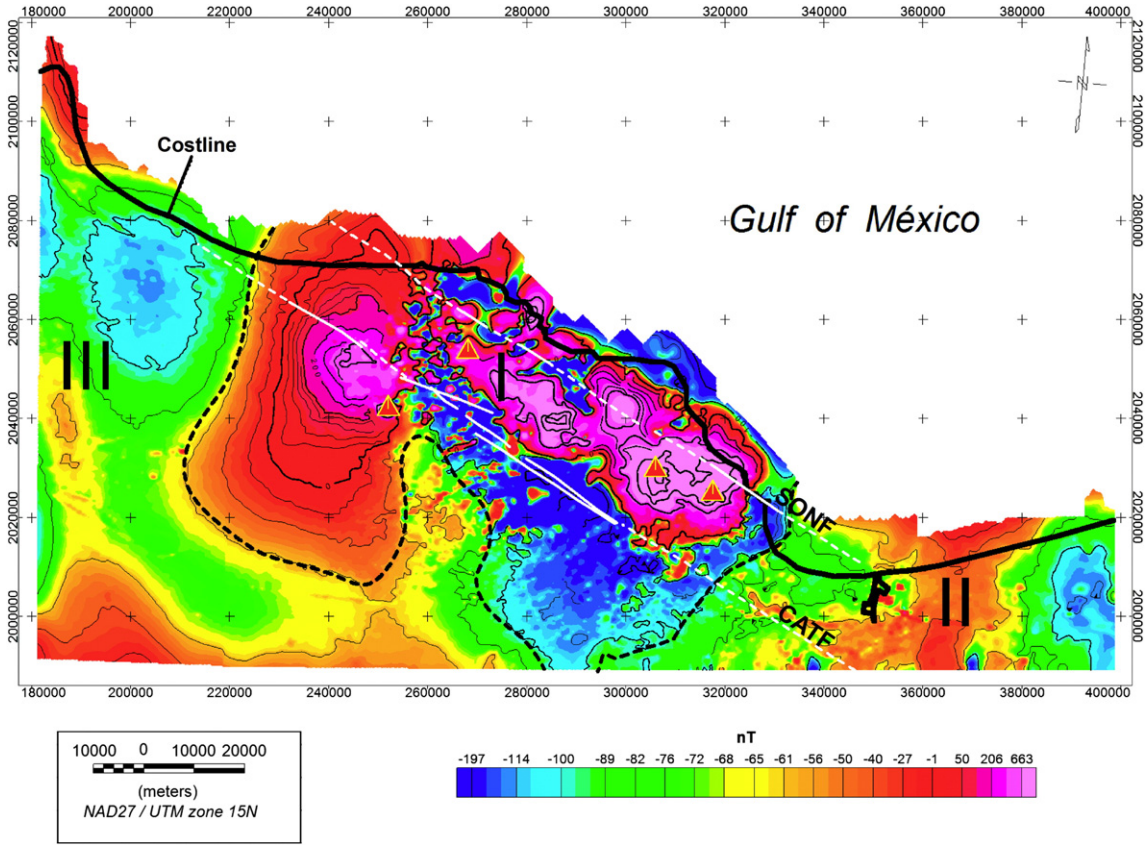

Fig. 8. Residual Magnetic Field reduced to the pole (RTP). Triangles: Main Volcanoes. (I II III): Magnetic Domains. Continuous lines: faults; dashed lines: inferred faults. CATF: Catemaco Fault. SONF: Sontecomapan Fault.
Modified after Andreani et al. (2008).

of the spectral power vs. wavenumber (***k***). All of the transformations were made using the commercial software Oasis Montaj from Geosoft Inc.

4.2. Inversion of the Bouguer gravity data

To obtain a density model fitting the gravimetric processed data, we used an inversion procedure developed by Rao et al. (1999). In this method, one considers that the gravity anomalies are due to heterogeneities of mass above a certain level. Rectangular prisms model the mass distribution with a given density contrast with the medium. The vertical attraction produced by each prism is computed at every grid point. The values obtained are compared with the observed values and iteratively optimized equating the differences to the algebraic sum of the products of the vertical gradients of gravity effects of prisms and increments to their thicknesses. Rao et al. (1999) include in their publication the Fortran codes to perform the described procedure; we used these codes to invert our gravity data.

The results of the inversion are given as depths to the top of the prisms in the grid. The values are placed at every grid point, which is the center of the prism, and contoured. We applied this method to both, the regional and residual, with a grid 26 × 16, corresponding to a spacing 8.4 × 8.2 km. For the average values of density of the intervening masses, we considered the estimates of Le Roy et al. (2007) based on offshore gravity and reflection profiles made NW from the TVF. Those values are 3300 kg/m^3 for the mantle, and 2750 kg/m^3 for the surrounding medium at the base of the crust while for the upper crust we considered a density of the surrounding medium of 2670 kg/m^3. Those values provide some constraints on the choice of densities, but given the simplicity of the model, which requires average densities for the main contrasting bodies, we proceeded by adjusting the density contrast until a good fit between observed and computed anomalies, in an area not affected by edge effects, was achieved.

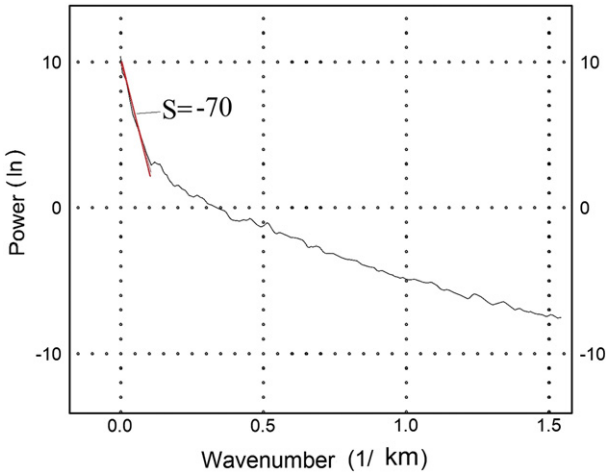

Fig. 9. a). Radial Power Spectrum of the Magnetic Field Reduced to the pole.

5. Results

5.1. Gravity and magnetic anomalies

The TVF shows conspicuous gravity and magnetic signatures covering roughly the same areas associated with the main volcanic lineaments and the largest volcanoes of the field. The gravity signature (Fig. 3) is an oblong positive anomaly with most of its extension on

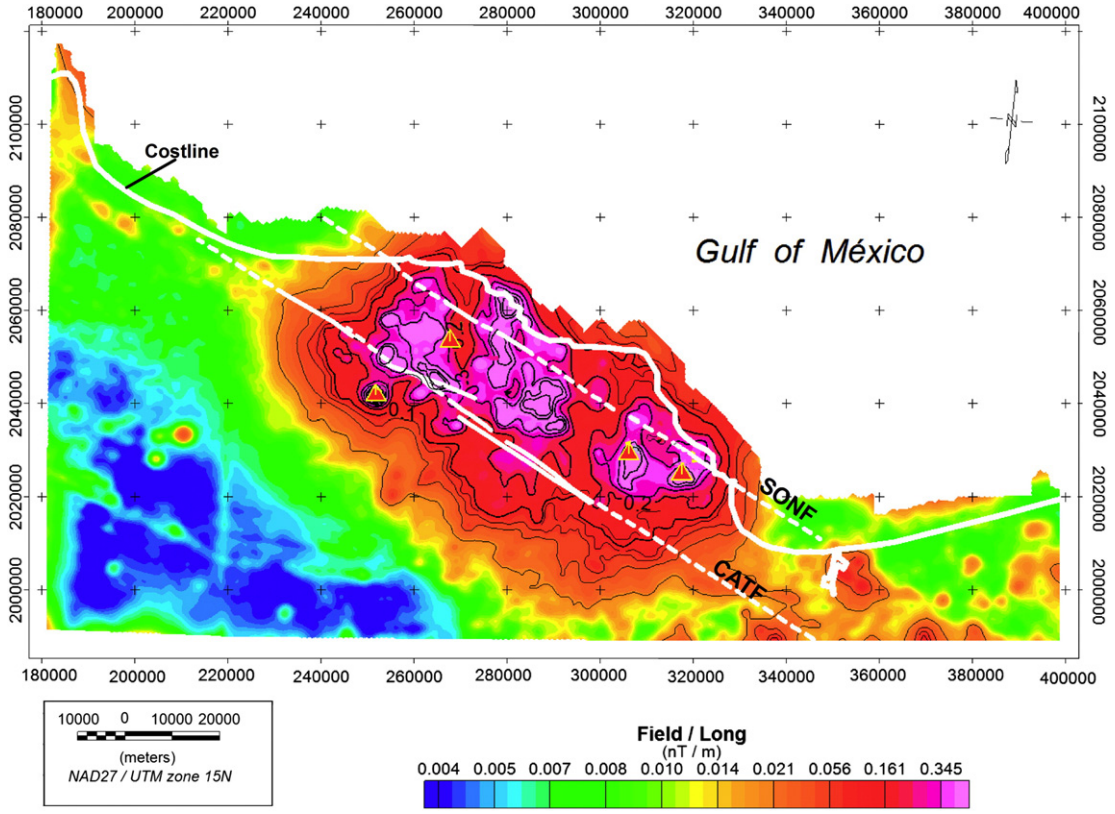

Fig. 10. Analytic Signal of the RMF continued 1 km upward. Triangles: Main Volcanoes Continuous lines: faults; dashed lines: inferred faults. CATF: Catemaco Fault. SONF: Sontecomapan Fault. Modified after Andreani et al. (2008).

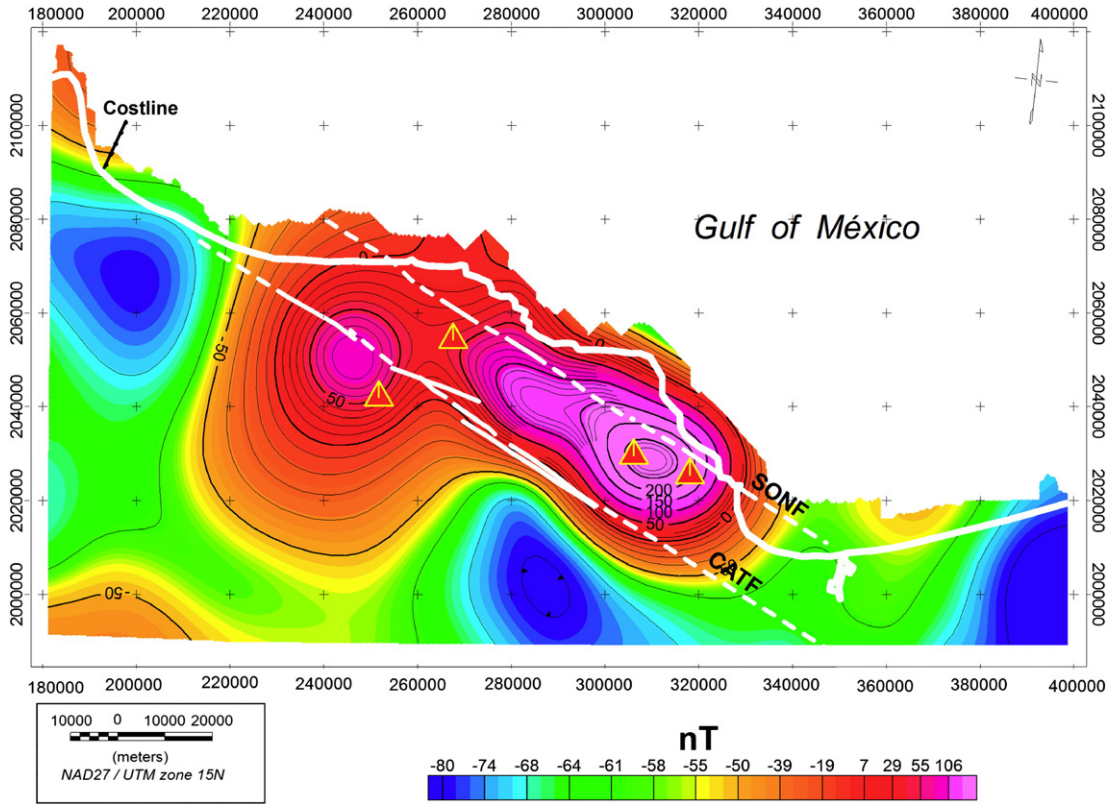

Fig. 11. Residual Magnetic Field reduced to the Pole continued 10 km upwards. Triangles: Main Volcanoes Continuous lines: faults; dashed lines: inferred faults. CATF: Catemaco Fault. SONF: Sontecomapan Fault.
Modified after Andreani et al. (2008).

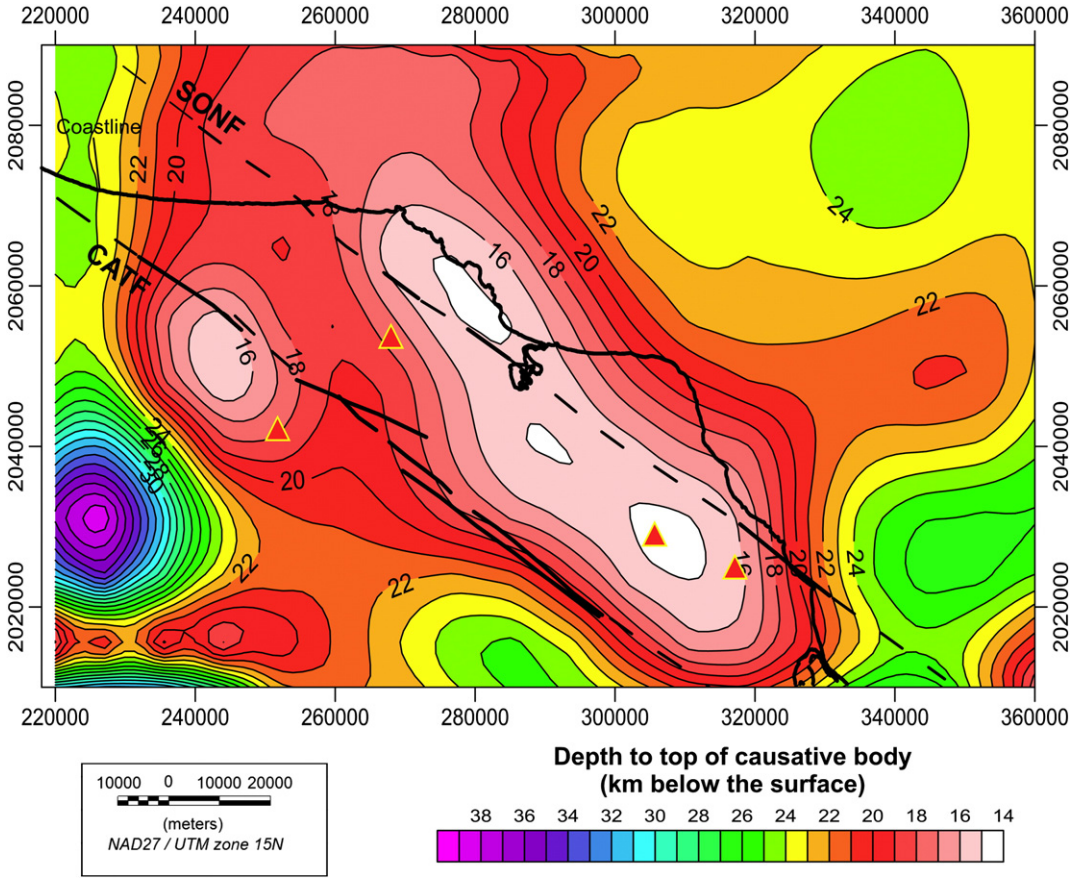

Fig. 12. Modeled depths to the interface between the high density and surrounding materials for the regional anomaly (contours in km below the surface). Triangles: Main Volcanoes Continuous lines: faults; dashed lines: inferred faults. CATF: Catemaco Fault. SONF: Sontecomapan Fault.
Modified after Andreani et al. (2008).

land although extending into the sea. The anomaly has a long axis oriented N40W and peaks at 135 mGal roughly at its center. From the peak values to the 0 mGal contour the anomaly is nearly 160 km long and 90 km wide with radial horizontal gradients averaging about 3 mGal/km. Fig. 4 shows the radial power spectrum of the Bouguer anomaly and the fitted straight line to the low frequencies. The average depth for small wavenumbers is about 29 km while for the residual the average value is about 7 km. These figures served as a guide to verify the separation regional-residual and the inversion of the data.

The regional component of the anomaly is also oblong with a long axis located roughly along the Sontecomapan Fault (Fig. 5). The excess mass related to the regional is of the order of 3.5×10^{16} kg. The long axis of the regional also approximates the direction of a lineament formed by the main volcanic centers in the TVF namely: San Martin Tuxtla, Santa Marta, and San Martin Pajapan, accompanied by several other cones. The Catemaco and Sontecomapan Faults also follow this direction (Andreani et al., 2008).

The residual shows four isolated anomalies with peaks close to the traces of the Catemaco and Sontecomapan Faults (Fig. 6). Three of the main volcanoes are located on the slopes of these positive anomalies. The exception is San Martin Tuxtla, the volcano that has been through the most recent stages of activity, is located close to a relative negative anomaly. The excess mass computed from the residual is 6×10^{15} kg.

The RMF (Fig. 7) shows the characteristic dipolar magnetic anomalies. To facilitate their interpretation in Fig. 8 we present the RTP. Fig. 9 displays the radial spectrum for the aeromagnetic data constructed from the RTP, which yields a depth to a causative body of about 5.8 km for the long wavelengths derived from the fitted straight line shown in the figure. The RTP indicates that the TVF is contained in a single aeromagnetic domain (AMD I), which extends in the NW–SE direction for about 116 km and is 61 km wide. It is made up of several magnetic anomalies with wavelengths varying from 1632 m to 6032 m (average 3354 m), and magnetic intensities ranging from 418 nT to 2245 nT, (average: 374 nT). It is also associated to horizontal gradients from −0.9318 nT/m to 0.7525 nT/m (average: −0.00017 nT/m). A comparison with the surrounding areas shows that they define magnetic domains albeit of very different characteristics (AMD II and AMD III). Fig. 10 displays the 1 km upward continuation of the AS showing more clearly the contours of superficial source bodies; with the main volcanoes appearing over the geomagnetic highs. Fig. 11 shows the RTP continued 10 km upwards, thereby highlighting the long period components of the magnetic signal. This anomaly covers an area overlapping the area covered by the regional gravity anomaly but differs in shape from the latter while their peaks do not coincide. Notice that the main volcanoes are close to the anomaly peaks but not at their summits.

In the RTP, the Santa Martha and San Martin Pajapan volcanoes are clearly associated with the same elongated source, trending WNW-ESE with a long and short axis 24 km and 14 km long, respectively. The estimated average depth is 7 km, and the intensity of magnetization varies from 2223 nT (Sta. Martha) to 1899 nT (San Martin Pajapan). The Cerro del Vigía volcano is located on the SE margin of a roughly circular anomaly with an average radius of 23 km. The summit of Cerro del Vigía is 1.6 km from the center of the anomaly and has an intensity of 1568 nT. San Martin Volcano lies 21 km to the NW of the center of an elongated anomaly about 23 km long and 9 km wide. The anomaly trends NW–SE with a magnetization of 509 nT.

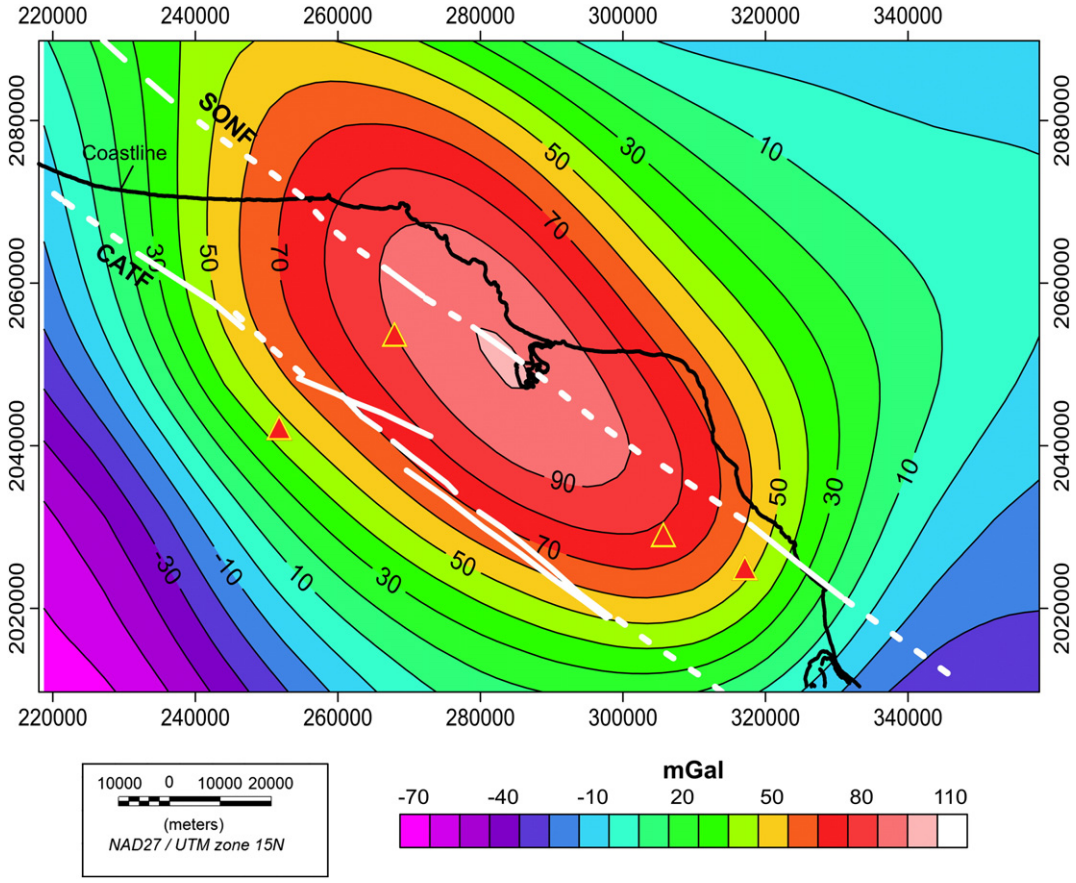

Fig. 13. Computed gravity anomaly after the inverted model of Fig. 12. Triangles: Main Volcanoes Continuous lines: faults; dashed lines: inferred faults. CATF: Catemaco Fault. SONF: Sontecomapan Fault
Modified after Andreani et al. (2008).

5.2. Inversion of Bouguer gravity data

Because of the inherent ambiguity in the models fitting data from potential fields, the first consideration concerns the depth to the anomaly's source. The gravity anomaly of the TVF is an isolated positive anomaly consisting largely of the regional. The residual is due to a mass of one order of magnitude smaller than the mass producing the regional as stated in the above section. Therefore, we consider first the depth to the source producing the regional. Since the TVF is covered by basaltic volcanic rocks, a look at the anomaly would lead to thinking that it is associated with such deposits. However, most of these materials were deposited during strombolian eruptions and consist of vesicular scoria, which due to the tropical weather in this region is highly altered; thus, its average density is not high in spite of its composition. This feature is in agreement with the results of Cordoba Montiel et al. (2014) who found anomalous slow velocities for surface waves at periods in the range 5 to 15 s, which suggests a medium of lower density in the upper crust. A more direct indication of the depth of the top of the source is provided by the radial spectrum of the anomaly, as stated in Section 5.1.

From the above considerations, we model the regional anomaly assuming an anomalous mass intruding above the 34 km Moho interface determined from Receiver Functions (Zamora-Camacho et al., 2010). Similarly for the residual, we assume bodies of contrasting density intruding above depths of 14 km. The density contrast that allowed a reasonable fit between observed and computed anomalies was 800 for the regional and 620 kg/m^3 for the residual. The inversion was performed at nodes far from the margins of the study area to avoid edge effects. Figs. 12 and 13 display the inverted density models and Figs. 14 and 15 the computed anomalies for the regional and residual, respectively. The average and standard deviation between the observed and computed anomalies for the regional is 1.38 mGal and a maximum absolute difference of 8.92 mGal. For the residual, we obtained 1.10 mGal and a maximum absolute difference of 1.53 mGal.

The model of the regional (Fig. 12) shows two main bodies. The largest is an elongated body 80 km long 20 km wide with an almost flat top 16 km deep, and gentle slopes falling to depths of 22 km. The major axis of the body is bent at the middle, which geographically coincides with the northern margin of the Catemaco Lake and the southern margin of the Young Series of Nelson and Gonzalez-Caver (1992). The north of the axis trends N30 W and its south N60 W. The latter is contained between the Sontecomapan and Catemaco Faults while the former continues from this area into the sea. Sierra Santa Martha and San Martin Pajapan are located on top of the major body while San Martin Tuxtla is placed on its slopes. The second body is an oval shaped body about 12 by 5 km in shape with its long axis oriented N30 W as well. Its top is 16 km deep, and Cerro Vigia lies about 12 km to the SW of the center of the body's top. The model of the residual (Fig. 13a) shows four isolated bodies nearly equant with tops 6 km deep. All of the large volcanoes are located at the projection on the surface of the slopes of the inferred bodies, which show summits situated close to the Catemaco and Sontecomapan Faults. The deepest parts of the bodies lie 20 km below the surface or about the depths of the lower body.

6. Discussion

The peculiarities of the TVF volcanic field are manifold. From a geophysical point of view, the gravity and geomagnetic signatures reveal the presence of a body of positive contrasting density that can

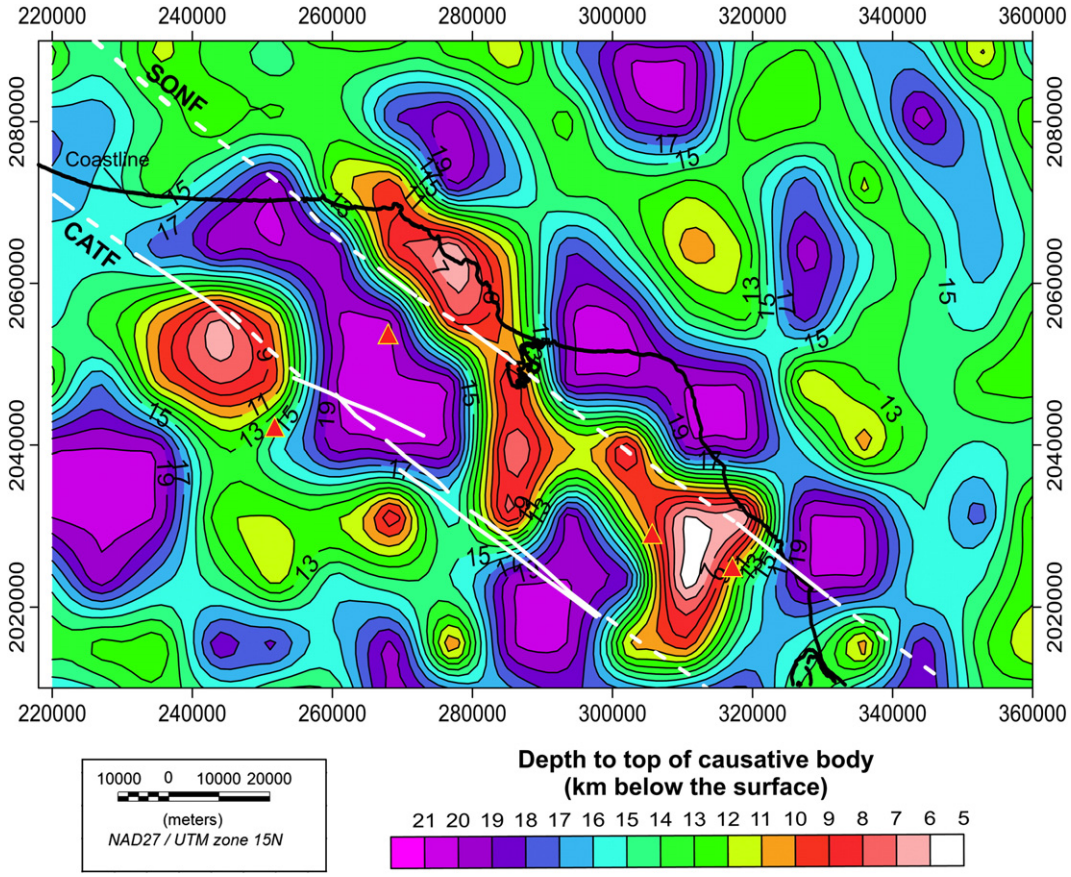

Fig. 14. Modeled depths to the interface between the high density and surrounding materials for the residual anomaly (contours in km below the surface). Triangles: Main Volcanoes Continuous lines: faults; dashed lines: inferred faults. CATF: Catemaco Fault. SONF: Sontecomapan Fault.
Modified after Andreani et al., (2008).

be interpreted as a magmatic intrusion. In this regard, it is worth considering the work of Thybo and Artemieva (2013) who, in their study of the geophysical evidence of underplating, remark that the latter was proposed as the process of magma ponding at the base of the crust as inferred from petrologic arguments. They considered that as a process of addition of high-density material to the lower crust, there is no difference between the traditional concept of underplated material and lower crustal magmatic intrusions. In their study, these authors give several examples of various tectonic environments. By and large, the presence of these bodies is revealed by seismic techniques but also from gravity data. Thus, in this sense, we suggest that the process at the TVF is that of underplating. This process not only adds material to the lower crust but also to the upper crust by different processes such as differentiation (Thybo and Artemieva, 2013). In addition to the evidence from the potential data, it is interesting to note that close to the shoreline at the TVF, outcrops of pillow lavas, probably of the old series, are exposed several tens of meters above mean sea level. These structures suggest uplifting of the area possibly due to the intrusion of magma at the base of the crust, a mechanism associated with underplating.

However, the sole presence of a magmatic body does not explain the characteristics of the volcanic field. The Veracruz Fault system also contributed to the construction of the TVF as proposed by Andreani et al. (2008). It is possible, however, that the participation of the fault system took place mainly in the upper part of the crust, which coincides roughly with the layer above the intracrustal interface determined by Zamora-Camacho et al. (2010). Two pieces of information suggest this interpretation; the first is the depth of the causative body found for the magnetic anomaly. This anomaly stems probably from the bottom of the upper crust, and the top of the lower intruding body where magma was distributed throughout the upper crust through the fault system and associated Riedel faults. In this context, it is worth noting that the distribution of cones in the TVF, in addition to the conspicuous NW-SE trending, also shows an E–W trend revealed by a rose diagram of vent alignments (Kobs-Nawotniak et al., 2010). The faults are weak zones that offer a path to the magma batches; even if not traveling through them, they can affect such paths as shown in analog laboratory experiments (Le Corvec et al., 2013a; Daniels and Menand, 2015). Thus, the summits of the gravity and long wavelength magnetic anomalies mark the site where the head of large magma batches have intruded into the crust. The conduits feeding the large volcanoes have been controlled subsequently by the fault system forming the volcanic edifices at some distance from the peaks in the signals.

The second fact is related to the research carried out in continental basaltic fields undergoing extension. These studies indicate that for those fields, the distribution of monogenetic vents is linked to the mechanical layering of the crust (Mazzarini, 2007). Thus, vents tend to cluster according to a power-law distribution defined over a range of lengths approximating the thickness of the fractured medium, which in many cases would correspond to the crust (Mazzarini, 2007). However, for the TVF an analysis of the fractal dimensions of vent spacing indicates that self-similarity holds over the search radii 0.8–12.6 km, indicating that the structures associated with magma rising are traceable to a depth of approximately 12.6 km (Kobs-Nawotniak et al., 2010). These depths are of the order of magnitude of the intracrustal interface found by Zamora-Camacho et al. (2010) and some 4 km above the top of the density anomaly modeled with the regional Bouguer anomaly. It is of interest to note that the depths inferred for the long wavelengths of the magnetic data are of the same order as those for

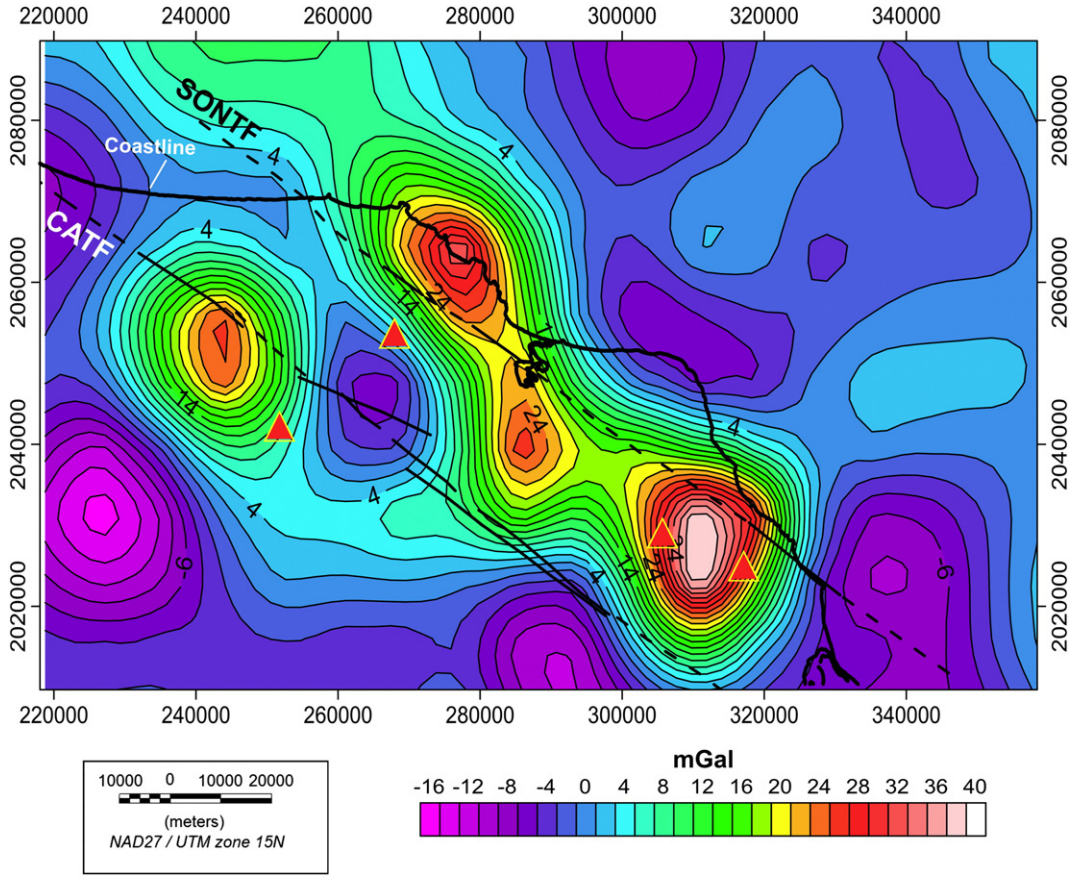

Fig. 15. Computed gravity anomaly after the inverted model of Fig. 14. Triangles: Main Volcanoes Continuous lines: faults; dashed lines: inferred faults. CATF: Catemaco Fault. SONF: Sontecomapan Fault.
Modified after Andreani et al. (2008).

the gravity residual, and both suggest that the distribution of the magma took place mostly through the upper crust. The major peaks in the magnetic and residual anomaly roughly coincide, but more detail is given by the aeromagnetic signal (for instance in the AS of Fig.10) because the susceptibility of the deposits is more contrasting than their density.

The role of the Veracruz fault system is not a surprising finding since it is known that the distribution of volcanoes is controlled not only by the availability of magma but also by the tectonic structures in the field. Such relationship has been proved in several volcanic fields (e.g. Tibaldi, 1995; Le Corvec et al., 2013b; Barde-Cabusson et al., 2014) and the case of the TVF can be added to these examples.

7. Conclusions

The gravity and geomagnetic anomalies from the TVF are circumscribed to the TVF. The regional component can be explained by a high-density density source body extending from the Moho to depths of about 16 km below sea level. The short wavelength positive gravity anomalies can be interpreted as due to shallow source bodies with tops about 6 km deep. These are probably the conduits feeding the principal volcanoes, which are located close to the peaks of the bodies. The short wavelength components of the magnetic anomalies also exhibit local maxima associated with the main volcanoes in the area. However, in the long wavelengths that prevail in the 10 km upper continuation of the RTP, the main volcanoes appear on the slopes of the maxima. The displacement between the highs in the long wavelength gravity and magnetic anomalies and the location of the large volcanoes suggest that the fault system strongly influences the emplacement of the volcanoes.

Acknowledgments

This work was funded by CONACyT, Mexico, via grant 428427-F and support to JME for a sabbatical leave that allowed its completion. The collaboration of Ms. Lourdes Godinez from Instituto de Geografía (UNAM) and Mr. David E. Torres Gaytán from IPICyT in the preparation of the figures is thankfully acknowledged. We also thank Drs. S.K. Singh, J. Yamamoto, and R. G. Martínez-Serrano for many useful discussions. We are very grateful to an anonymous reviewer and Dr. Jochen Kamm, for their detailed and constructive comments, which significantly improved this paper.

Appendix A. Supplementary data

Supplementary data to this article can be found online at http://dx.doi.org/10.1016/j.jvolgeores.2016.05.006.

References

Aguilera Gómez, L., 1988. Petrología de Las Rocas ígneas del área de Los Tuxtlas, Veracruz (Tesis Profesional) Instituto Politécnico Nacional, Mexico (58 pp.).
Andreani, L., Rangin, C., Martínez-Reyes, J., Le Roy, C., Aranda-García, M., Le Pichon, X., Peterson-Rodriguez, R., 2008. The Neogene Veracruz fault: evidences for left-lateral slip along the southern Mexico block. Bull. Soc. Géol. Fr. 179, 195–208.
Barde-Cabusson, S., Gottsmann, J., Martí, J., Bolós, X., Camacho, A.G., Geyer, A., Planagumà, L., Ronchin, E., Sánchez, A., 2014. Structural control of monogenetic volcanism in the Garrotxa volcanic field (Northeastern Spain) from gravity and self-potential measurements. Bull. Volcanol. 76 (1), 788. http://dx.doi.org/10.1007/s00445-013-0788-0.
Blakely, R.J., 1996. Potential Theory in Gravity and Magnetic Applications. Cambridge University Press, Cambridge, U.K.
Cantagrel, J., Robin, C., 1979. K–Ar dating on eastern Mexican volcanic rocks: relations between the andesitic and alkaline provinces. J. Volcanol. Geotherm. Res. 5, 99–114.

Cordoba Montiel, F., Iglesias Mendoza, A., Singh, S.K., Spica, Z., Legrand, D., 2014. Grupo de Ondas de Rayleigh Para el Oriente de México y el Istmo de Tehuantepec. Bol. Soc. Geol. Mex. 66, 441–457.

Daniels, K.A., Menand, T., 2015. An experimental investigation of dyke injection under regional extensional stress. J. Geophys. Res. Solid Earth 120. http://dx.doi.org/10.1002/2014JB011627.

De la Fuente, M., Mena, M., Aiken, C., 1994. Cartas Gravimétricas de la Republica Mexicana. Instituto de Geofísica, UNAM, Mexico.

Dimitriadis, K., Tselentis, G.A., Thanassoulas, K., 1987. Basic program for 2-D spectral analysis of gravity data and source-depth estimation. Comput. Geosci. 13 (5), 549–560.

Espíndola, V.H., 2009. Modelos de Velocidad Cortical Utilizando Funciones de Receptor Aplicado a Estaciones de Banda Ancha del SSN, Mexico (Ph. D. Thesis) UNAM, México.

Espindola, J.M., Zamora-Camacho, A., Godinez, M.L., Schaaf, P., Rodriguez-Elizarraras, S., 2010. The 1793 eruption of San Martin Tuxtla volcano, Veracruz, México. J. Volcanol. Geotherm. Res. 197, 188–208.

Ferrari, L., Orozco-Esquivel, M.T., Manea, V., Manea, M., 2012. The dynamic history of the trans-Mexican Volcanic Belt and the Mexico subduction zone. Tectonophysics 522-523, 122–149. http://dx.doi.org/10.1016/j.tecto.2011.09.018.

Kim, Y.H., Clayton, R.W., Keppie, F., 2011. Evidence of a collision between the Yucatán block and Mexico in the Miocene. Geophys. J. Int. 187, 989–1000.

Kobs-Nawotniak, S.E., Espíndola, J.M., Godinez, M.L., 2010. Spatial Statistical Survey of the Tuxtla Volcanic Field (TVF), Veracruz, Mexico. Union Geofisica Mexicana, Reunión Anual 2010, Puerto Vallarta, Jal., Mexico.

Le Corvec, N., Menand, T., Lindsay, J., 2013a. Interaction of ascending magma with pre-existing crustal fractures in monogenetic basaltic volcanism: an experimental approach. J. Geophys. Res. Solid Earth 118, 1–17. http://dx.doi.org/10.1002/jgrb.50142.

Le Corvec, N., Menand, T., Bernhard Spörli, K., Rowland, J., Lindsay, J., 2013b. Spatial distribution and alignments of volcanic centers: clues to the formation of monogenetic volcanic fields. Earth Sci. Rev. 124, 96–114.

Le Roy, C., Rangin, C., Le Pichon, X., Ngoc, H.N.T., Andreani, L., Aranda-García, M., 2007. Neogene crustal shear zone along the western Gulf of Mexico margin and its implications for gravity sliding processes. Evidences from 2D and 3D multichannel seismic data. Bull. Soc. Géol. Fr. 178, 175–185.

Mazzarini, F., 2007. Vent distribution and crustal thickness in stretched continental crust: the case of the afar depression (Ethiopia). Geosphere 3, 152–162. http://dx.doi.org/10.1130/GES00070.1.

Melgar, D., Perez-Campos, X., 2010. Imaging the Moho and subducted oceanic crust at the isthmus of Tehuantepec, Mexico, from receiver functions. Pure Appl. Geophys. 168, 1449–1460.

Moore, G.W., Del Castillo, L., 1974. Tectonic evolution of the southern Gulf of Mexico. Geol. Soc. Am. Bull. 85, 607–618.

Nelson, S.A., Gonzalez-Caver, E., 1992. Geology and K–Ar dating of the Tuxtla volcanic field, Veracruz, Mexico. Bull. Volcanol. 55, 85–96.

Nelson, S.A., Gonzalez-Caver, E., Kyser, T.K., 1995. Constraints on the origin of alkaline and calc-alkaline magmas from the Tuxtla volcanic field, Veracruz, Mexico. Contrib. Mineral. Petrol. 122, 191–211.

Padilla y Sánchez, R.J., 2007. Evolución geológica del sureste mexicano desde el Mesozoico al presente en el contexto regional del Golfo de México. Bol. Soc. Geol. Mex. 59, 19–42.

Pal, P.C., Khurana, K.K., Unnikrishnan, P., 1979. Two Examples of Spectral Approach to Source Depth Estimation in Gravity and Magnetics. Pageoph Vol. 117 (78/79). Birkhaüser-Verlag, Basel.

Pichler, H., Weyl, R., 1976. Quaternary alkaline volcanic rocks in eastern Mexico and Central America. Munster. Forsch. Geol. Paläont. 38/39, 159–178.

Prost, G., Aranda-Garcia, M., 2001. Tectonics and hydrocarbon systems of Veracruz Basin, Mexico. In: Bartolini, C., Buffler, R.T., Cantu-Chapa, A. (Eds.), The Western Gulf of Mexico Basin. Tectonics, Sedimentary Basins and Petroleum Systems. AAPG Memoir Vol. 75, pp. 271–291.

Rao, P.R., Swamy, K.V., Radhakrishna Murthy, I.V., 1999. Inversion of gravity anomalies of three-dimensional density interfaces. Comput. Geosci. 25, 887–896.

Rios Macbeth, F., 1952. Estudio geológico de la región de Los Tuxtlas. Bol. Soc. Mex. Geol. Petrol. 4, 315–377.

Robin, C., 1976. Prèsence simultanèe de magmatismes de significations tectoniques opposèes dans l'Est du Mexique. Bull. Soc. Geol. Fr. 18, 1637–1645.

Sawyer, D.S., Buffler, R.T., Pilger, R.H., 1991. The crust under the Gulf of Mexico Basin. In: Salvador, A. (Ed.), The Gulf of Mexico Basin: Boulder, Colorado, Geological Society of America, Geology of North America, J, pp. 53–72.

Spector, A., Grant, F.S., 1970. Statistical models for interpreting aeromagnetic data. Geophysics 35 (2), 293–302.

Thorpe, R.S., 1977. Tectonic significance of alkaline volcanism in eastern Mexico. Tectonophysics 40, T19–T26.

Thybo, H., Artemieva, I.M., 2013. Moho and magmatic underplating in continental lithosphere. Tectonophysics 609, 605–619.

Tibaldi, A., 1995. Morphology of pyroclastic cones and tectonics. J. Geophys. Res. 100 (B12), 24521–24,535.

Verma, S.P., 2006. Extension related origin of magmas from a garnet-bearing source in Los Tuxtlas volcanic field, Mexico. Int. J. Earth Sci. 95, 871–901.

Zamora-Camacho, A., Espindola, V.H., Pacheco, J.F., Espindola, J.M., Godinez, M.L., 2010. Crustal thickness at the Tuxtla volcanic field (Veracruz, Mexico) from receiver functions. Phys. Earth Planet. Inter. 182, 1–9.